

Mathematical modeling of human brain physiological data

Matthias Böhm,^{1,2,*} Rupert Faltermeier,² Alexander Brawanski,² and Elmar W. Lang¹
¹*CIML Group, Department of Biophysics, University of Regensburg, 93040 Regensburg, Germany*
²*Department of Neurosurgery, University Hospital Regensburg, 93042 Regensburg, Germany*
 (Received 24 June 2013; published 10 December 2013)

Recently, a mathematical model of the basic physiological processes regulating the cerebral perfusion and oxygen supply was introduced [Jung *et al.*, *J. Math. Biol.* **51**, 491 (2005)]. Although this model correctly describes the interdependence of arterial blood pressure (ABP) and intracranial pressure (ICP), it fails badly when it comes to explaining certain abnormal correlations seen in about 80% of the recordings of ABP together with ICP and the partial oxygen pressure (TiPO₂) of the neuronal tissue, taken at an intensive care unit during neuromonitoring of patients with a severe brain trauma. Such recordings occasionally show segments, where the mean arterial blood pressure is *correlated* with the partial oxygen pressure in tissue but *anticorrelated* with the intracranial pressure. The origin of such abnormal correlations has not been fully understood yet. Here, two extensions to the previous approach are proposed which can reproduce such abnormal correlations in simulations quantitatively. Furthermore, as the simulations are based on a mathematical model, additional insight into the physiological mechanisms from which such abnormal correlations originate can be gained.

DOI: 10.1103/PhysRevE.88.062711

PACS number(s): 87.19.L-, 87.85.Tu

I. INTRODUCTION

Mathematical modeling of the cerebral physiology has to cope with two major problems, namely, the complexity of the system itself and the verification of the modeling results by appropriate measurements. As described by the *Monroe Kelly* doctrine, the intracranial space can be seen as a closed system, confined within the nearly rigid skull. This property exacerbates elaborate measurements, especially if long-term observations are needed. Despite considerable progress in neuroimaging and the so called multimodal monitoring implemented at many neurosurgical intensive care units, the validation of such models is still challenging. Hence most of the modeling approaches focus on a view of specific properties of the cerebral physiology and the associated measurements. In the following, we present a, not necessarily comprehensive, summary of the variety of modeling approaches and the different problems they address.

A. A short literature survey

In 1973 Marmarou [1,2] introduced a mathematical model of cerebrospinal fluid (CSF) pressure-volume compensation. In the 1980s the concept of a vascular component of the intracranial pressure (ICP) was proposed, and it was shown that in cases of traumatic brain injuries only 30% of an elevated ICP could be explained by changes in CSF circulation, while the remaining 70% had to be attributed to the vascular ICP component.

In 1988, Ursino [3,4] proposed more elaborate hydrodynamic models of CSF fluid dynamics. Later, a simple mathematical model of the interaction between ICP and cerebral haemodynamics has been presented [5,6]. It included the hemodynamics of the arterial-arteriolar cerebrovascular bed, CSF production, and reabsorption processes, and the nonlinear pressure-volume relationship of the craniospinal compartment. The model was used to simulate interactions between ICP,

cerebral blood volume (CBV), and autoregulation. Simulation results suggested an instability of ICP dynamics in patients with elevated CSF outflow resistance and decreased intracranial compliance, provided cerebral autoregulation is efficient. Subsequently, intracranial pressure dynamics in patients with acute brain damage have been modeled also by Ursino *et al.* [6]. A simple mathematical model was used to analyze the time pattern of ICP during pressure-volume index (PVI) tests. A satisfactory fitting between model response and patient data was achieved by adjusting the CSF outflow resistance, the intracranial elastance coefficient ($1/C$), and the gain and time constant of cerebral autoregulation. The results showed that in cases of weak autoregulation, ICP mainly reflects CSF circulation and passive cerebral blood volume changes. These models were later completed by including CO₂ reactivity and CO₂ pressure changes [7,8]. More recently, a physiological model of cerebral blood flow control is presented by [9] and extensively discussed in the thesis of Tachtsidis [10].

The work of Lakin [11] revoked the Monro-Kellie doctrine and developed a mathematical model for the dynamics of intracranial pressures, volumes, and flows that embedded the intracranial system in extensive whole-body physiology. The model consistently introduced compartments representing the tissues and vasculature of the extradural portions of the body, including both the thoracic region and the lower extremities. In addition to vascular connections, a spinal-subarachnoid CSF compartment bridged intra- and extracranial physiology allowing explicit buffering of intracranial pressure fluctuations by the spinal cord. The model contained cerebrovascular autoregulation, regulation of systemic vascular pressures by the sympathetic nervous system, regulation of CSF production in the choroid plexus, a lymphatic system, colloid osmotic pressure effects, and realistic descriptions of cardiac output.

Wakeland and Goldstein [12] presented a computer model of intracranial pressure dynamics during traumatic brain injury that explicitly models fluid flows and volumes. The response to changes in clinical parameters was monitored through key characteristics such as hematoma volume and CSF uptake resistance. The estimated values for hematoma volume and

*matthias.boehm@ur.de

other subject characteristics were plausible but could not be verified empirically.

A further mathematical model of blood, cerebrospinal fluid, and brain dynamics has been proposed by Linninger *et al.* [13]. Using first principles of fluid and solid mechanics, the compartmental model, including blood, CSF, brain parenchyma, and the spinal canal, predicted intracranial pressure gradients, and blood and CSF flows and displacements under normal and pathological conditions. Fluid-solid interactions of the brain parenchyma with cerebral blood and CSF are calculated. The model provides the transitions from normal dynamics to the diseased state. Predicted results were compared with physiological data from cine phase-contrast magnetic resonance imaging [14] to verify the dynamic model.

Moppett *et al.* [15] presented a lumped parameter model for time-dependent simulation of the cerebral blood flow (CBF) and metabolism including the cerebral oxygenation, and the carbon dioxide content and pH of cerebral blood.

Masoumi *et al.* [16] studied a mathematical model of CSF pulsatile hydrodynamics based on fluid-solid interactions. This study considered a fluid-solid interaction model of CSF hydrodynamics in the ventricular system based on clinical data as arterial blood pressure (ABP), ICP, and the venous blood pressure (VBP). In addition, the model has been modified by considering CSF pulsatile production rate as the major factor of CSF motion. The resulting CSF flow pattern, ICP distribution, and velocity magnitude were in good agreement with published models and cine magnetic resonance imaging (cineMRI) experiments, respectively.

Sweetman *et al.* [17] presented a three-dimensional model of human CSF spaces by reconstructing patient-specific brain geometries from magnetic resonance images (MRI). The model was validated by comparing the predicted flow rates with cine phase-contrast MRI measurements.

Online estimation of cerebral autoregulation (CA) was studied by Aoi *et al.* [18]. The authors used data from transcranial Doppler and high resolution ABP measurements to frame the assessment of CA as a parameter estimation problem, in which they estimated the parameters of a nonlinear mathematical model of CA using an ensemble Kalman filter (EnKF). The latter allowed one to estimate the parameters of a model of cerebral hemodynamics which predicted intracranial pressure and cerebral blood flow velocity, generated from real patient arterial blood pressure measurements.

Kashif *et al.* [19] recently introduced a noninvasive determination of ICP based on measurements of peripheral ABP and blood flow velocity (BFV) in the middle cerebral artery (MCA), both at intraheartbeat resolution. A physiological model of cerebrovascular dynamics provides mathematical constraints that relate the measured wave forms to ICP. The algorithm produced patient-specific ICP estimates with no calibration or training. The achieved accuracy is already comparable to that of some invasive ICP measurement methods in current clinical use.

B. The hemodynamical and oxygen transport model

In Jung *et al.* [20] a simple compartmental approach, based on the work of Ursino *et al.* [5] was proposed to design a mathematical model for the interpretation of

multimodal neuromonitoring data, recorded at a neurosurgical intensive care unit. It is used to study the impact of defective cerebral regulatory systems, such as cerebral autoregulation and cerebral compliance, on continuously measured data such as ABP, ICP, and the partial oxygen pressure of brain tissue ($TiPO_2$). The above mentioned regulatory systems show certain dysfunctions in patients with a severe brain trauma whose origins are not well understood yet. The key functional role of these systems is the maintenance of an adequate supply of the human brain with oxygen and nutrition. Any dysfunction may have a dramatic impact on the patient's health status. For these reasons the proposed model attributes special attention to the cerebral compliance, i.e., the ability of the brain to compensate intracranial volume changes, by modeling a pressure dependent CSF production and absorption. Furthermore, the cerebral autoregulation, modeled as a nonlinear resistance, is dynamically adapted to a changing ABP by a control parameter α which allows the simulation of different levels of autoregulation failures. Additionally, an extra storage compartment was added to simulate an evolving brain swelling, one of the most frequent complications arising during treatment of severe brain traumata. Such a swelling may lead to a diminished cerebral compliance with distinct impact on the intracranial pressure. A detailed description of this simple model, called the HOM model in the following, and related simulation results are given in [20], where HOM is an abbreviation for hemodynamical and oxygen transport model.

II. MODELING APPROACH

As already mentioned in this study a compartmental approach is used to model cerebral perfusion. The complex physiological structures of the human brain are subdivided into seven different functional subunits, where every subunit is described by its physical properties. The used compartments characterize the functionality of the arteries, veins, capillaries, brain tissue, sagittal sinus, cerebrospinal fluid, and the cranial bone. Additionally an extra compartment E is used to simulate swelling of the brain. For a more detailed description, see [20]. As a starting point, the conservation of mass is used including that a change of mass accounts for a change in density and/or change in volume of a compartment:

$$\sum q_i = \frac{dm}{dt} = \underbrace{\frac{\partial m}{\partial \rho}}_{=V} \frac{\partial \rho}{\partial t} + \underbrace{\frac{\partial m}{\partial V}}_{=\rho} \frac{\partial V}{\partial t}. \quad (1)$$

Here, the following physiological assumptions were made: Blood and CSF are considered incompressible media, whereas the brain tissue is considered a compressible medium. All fluxes are considered stationary, more specifically blood flow is considered to be laminar. The Hagen-Poiseuille law is then used to describe the flow q_{XY} between two compartments X and Y :

$$q_{XY} = \frac{\Delta p_{XY}}{R_{XY}} = \frac{p_X - p_Y}{R_{XY}}. \quad (2)$$

The volume change of a compartment can be modeled by assigning a compliance $C(\varphi)$ to compartments surrounded by

an elastic membrane:

$$V - V_0 = \int_0^p C(\varphi) d\varphi \quad \text{with } p = p_{\text{ext}} - p_{\text{int}}. \quad (3)$$

As the cranial bone of the human head acts as a closed compartment, the total volume change of all compartments has to be zero:

$$\sum_i \dot{V}_i = 0. \quad (4)$$

For modeling the resistance of all blood vessels, the Hagen-Poiseuille law can be used:

$$R_{XY} = \frac{k'_R}{r^4} = \frac{k_R}{V^2}. \quad (5)$$

In this framework, the cerebral autoregulation will be modeled via temporal variations of the compliance C_{AB} :

$$R_{AC} = \frac{k'_{RAC}}{r^4} = \frac{k_{RAC}}{V_A^2} = \frac{k_{RAC}}{C_{AB}^2(p_A - p_B)^2}, \quad (6)$$

whereas $k_{RAC} = \text{const}$ and $V_A = C_{AB}(p_A - p_B)$. Compliance dynamics $\partial_t C_{AB}$ is given by

$$\frac{dC_{AB}(t)}{dt} = -\frac{1}{\tau} [C_{AB}(t) - C_{AB\text{reg}}(\alpha x)] \quad (7)$$

with

$$x = \frac{q_{AC} - q_{AC_n}}{q_{AC_n}}, \quad (8)$$

whereas q_{AC} equals the cerebral blood flow and $q_{AC_n} = \text{const}$ describes the CBF required for the standard tissue metabolism. The degree of autoregulation is given by α and τ is the time constant of the regulation. The regulation term $C_{AB\text{reg}}$ itself has the following form, which is proposed by Ursino and Lodi in [5]:

$$C_{AB\text{reg}}(\alpha x) = C_{ABn} - \Delta C_{AB} \tanh\left(\frac{\alpha x}{\Delta C_{AB}}\right). \quad (9)$$

Thereby ΔC_{AB} represents the maximum gain for the autoregulation and C_{ABn} is the compliance of the arteries for the standard CBF. As the autoregulation curve is not symmetrical, ΔC_{AB} assumes different values for dilation ($x < 0$) and constriction ($x > 0$):

$$\Delta C_{AB} = \begin{cases} \Delta C_{AB1}, & x < 0 \\ \Delta C_{AB2}, & x > 0. \end{cases} \quad (10)$$

The brain tissue is surrounded by the so-called cerebrospinal fluid. This fluid is produced at a capillary level and (mainly) absorbed at the sagittal sinus. The driving forces of production and absorption are the pressure differences between capillaries and the CSF compartment, and between the CSF compartment and the sagittal sinus, respectively:

$$q_{CF} = \frac{p_C - p_B}{R_{CF}} \quad \text{and} \quad q_{FS} = \frac{p_B - p_S}{R_{FS}}. \quad (11)$$

The sagittal sinus is a stiff vessel and therefore does not collapse in cases of a negative pressure gradient between the outside and inside. Additionally, it should be mentioned, that a

reversal of both fluxes is not possible. The lacking compliances C_{VB} and C_B are described by

$$C_{VB} = \frac{1}{k_V[\sqrt{(p_V - p_B)^2} + p_{V_0}]} \quad (12)$$

and

$$C_B(p_B) = \frac{1}{k_B(|p_B| + p_{B_0})}, \quad (13)$$

whereas k_V , p_{V_0} , k_B , and p_{B_0} are constant.

Combining the above mentioned fluxes and compliances via the mass conservation leads to a set of differential equations similar to Eqs. (16)–(22), but only describing a one hemispheric model.

Although this model could reliably reproduce the primary experimental observations such as the autoregulation curve and the pressure volume curve, it badly failed to reproduce abnormal correlations of ABP vs ICP and TiPO₂, which were detected recently [21] in multimodal neuromonitoring data (see Figs. 6 and 7). To rectify these deficiencies of the simple HOM model, two extensions will be added which include a two hemisphere model and incorporate a Starling resistor into the venous compartment. These extensions, resulting in a model henceforth called esHOM, precisely reproduce the observed abnormal correlations mentioned above and provide clues to their possible physiological origin.

III. THE EXTENDED HOM MODEL

In the following, two extensions to the HOM model are proposed, which reflect two additional physiological characteristics of the human brain, namely, the compressibility of the venous compartment and the existence of two hemispheres.

A. Two hemispheres

In order to better reflect the structure of the human brain, a splitting of the model into a left and right hemisphere is proposed. Further, this splitting allows modeling the autoregulation independently in both hemispheres and therefore allows simulating a *local* failure of the autoregulation in only one of the two hemispheres. Such situations may arise during a severe brain injury.

In Fig. 1 a schematic representation of the two hemisphere model is shown (compare [20] for the schematic representation of the HOM model). Here, extra compartments for the arteries (A), capillaries (C), and veins (V) are added, whereas both venous compartments empty into the sagittal sinus (S). In

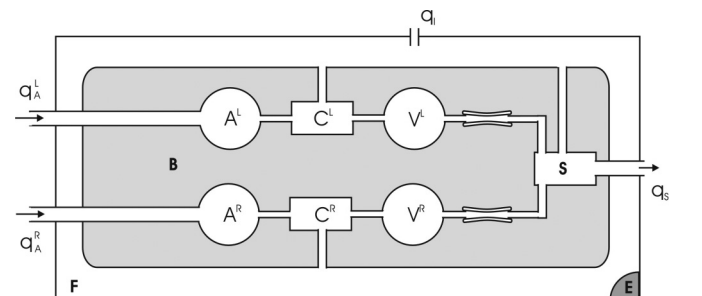


FIG. 1. Schematic view of compartment model.

addition, the model contains two inflows q_A^i (the superscript “ i ” denotes the left (L) and the right (R) hemisphere of a human brain), which represent the inflows of blood into each of the two hemispheres. As depicted in Fig. 1, both hemispheres contribute to the CSF production.

The new nonlinear system of differential equations can be solved numerically and will be given in a following section.

B. Starling resistor

One deficiency of the HOM model lies in its imperfect specification of the venous compartment. Because of the elastic properties of the venous blood vessels, in cases of a diminished cerebral compliance, the venous system can collapse. Such a behavior can be modeled by describing the resistance of the veins via a Starling resistor, as proposed in [7]. Thereby, the resistance of the veins depends on the pressure differences between veins and sagittal sinus, and veins and pressure inside the brain:

$$R_{VS} = \begin{cases} \frac{1}{g_{VS}} \frac{p_V - p_S}{p_V - p_B} & \text{if } (p_V - p_B) > 0 \\ \infty & \text{else,} \end{cases} \quad (14)$$

where by g_{VS} the conductance between veins and sinus is given. For the case where the ICP is higher than the pressure inside the veins, the system collapses and the resistance tends towards infinity.

The compliance of the veins, which describes the volume change with respect to the pressure difference between pressure inside the veins and brain tissue, can then be calculated according to

$$C_{VB} = \frac{V_V}{p_V - p_B}. \quad (15)$$

Here V_V denotes the volume of the veins. The resulting model, which, in addition to modeling two hemispheres, incorporates the Starling resistor, is called the esHOM model henceforth.

C. Differential equation system

Combining all aforementioned features, the model is defined by the following set of differential equations:

$$\dot{V}_E = q_E, \quad (16)$$

$$\dot{V}_F = \sum_i \frac{p_C^i - p_B}{R_{CF}^i} + q_I + \frac{p_S - p_B}{R_{FS}}, \quad (17)$$

$$\dot{V}_V^i = \frac{p_C^i - p_V^i}{R_{CV}^i} + \frac{p_S - p_V^i}{R_{VS}^i}, \quad (18)$$

$$\dot{C}_{AB}^i = \frac{1}{\tau} C_{ABreg}^i - C_{AB}^i, \quad (19)$$

$$\dot{p}_B = \frac{1}{C_B + \sum_i C_{AB}^i} \left\{ \sum_i [\dot{C}_{AB}^i (p_A^i - p_B) + \dot{V}_V^i + C_{AB}^i \dot{p}_A^i] + \dot{V}_F + \dot{V}_E \right\}, \quad (20)$$

$$\dot{p}_V^i = \dot{p}_B + \frac{\dot{V}_V^i}{C_{VB}^i} \quad (21)$$

with

$$C_{ABreg}^i = C_{ABn} - \Delta C_{AB} \tanh \left[\alpha \left(1 - \frac{q_{AC}^i}{q_{ACn}} \right) \right]. \quad (22)$$

IV. EXPERIMENTAL SETUP

In order to reproduce the observed interdependencies of the data, the general behavior of both models, HOM and esHOM, need to be known. Therefore we present simulations of the changes in ICP and TiPO₂ resulting from varying the ABP under different physiological conditions. A possible successive failure of the cerebral control mechanisms can be simulated by means of four different scenarios:

Case 1. Active autoregulation, sufficient compliance.

Case 2. Inactive autoregulation, sufficient compliance.

Case 3. Active autoregulation, insufficient compliance.

Case 4. Inactive autoregulation, insufficient compliance.

The first scenario represents an optimal condition for a patient. In the second scenario, the autoregulation is inactive, e.g., due to a severe head trauma. In the third and fourth scenario, additionally a swelling of the brain occurs, hence the fourth scenario represents the worst case.

For case 1 and case 2, both models produce very similar results (compare [22] for graphs). In case 1, the experimentally known behavior of the autoregulation is well reproduced. In case 2, the expected, roughly linear, increase of TiPO₂ along with a moderate increase of ICP can be reproduced as well, though not quantitatively.

In the following we will discuss the behavior of ICP and TiPO₂ as predicted by the HOM and esHOM models with respect to the above mentioned four scenarios.

A. HOM

In Fig. 2, the graphs for case 3 (solid lines) are plotted with reference to case 1 (dashed lines). In both cases, the autoregulation mechanism is fully functional ($\alpha = 2.0$).

In cases of a swelling (case 3), a small drop of the TiPO₂ occurs inside an ABP interval ranging from 67 (hPa) to 113 (hPa) contrary to the case of no swelling (case 1). The main difference between both simulations lies in an altered ICP dynamics inside an ABP interval between 67 (hPa) and

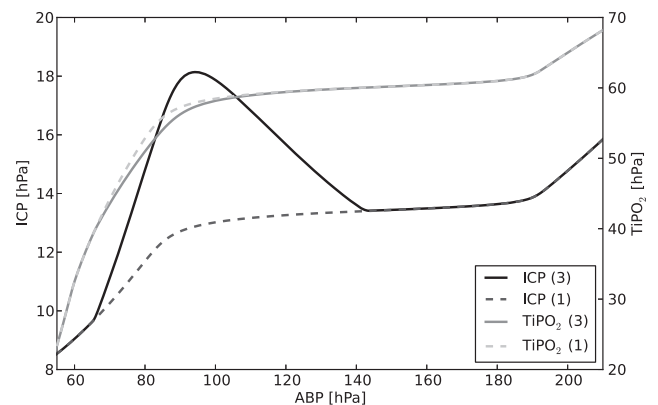


FIG. 2. TiPO₂ and ICP against ABP for $\alpha = 2.0$, $V_E = 0$ (ml) (case 1) and $V_E = 30$ (ml) (case 3); HOM.

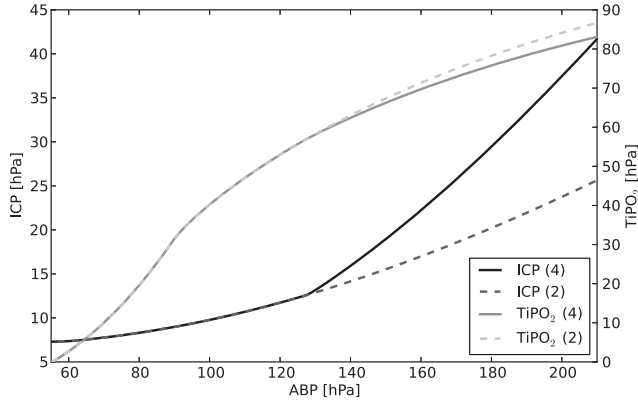


FIG. 3. $TiPO_2$ and ICP against ABP for $\alpha = 0.0$, $V_E = 0$ (ml) (case 2) and $V_E = 30$ (ml) (case 4); HOM.

140 (hPa). Due to brain swelling [$V_E = 30$ (ml)], the ICP shows a strong overshoot when compared to case 1 and the ICP maximum is reached at an ABP of ~ 93 (hPa) just when the autoregulation plateau begins in case 1.

For the scenarios where the autoregulation is disabled ($\alpha = 0.0$) the corresponding ICP and $TiPO_2$ responses are depicted in Fig. 3. The graphs for case 4 (solid lines) are compared with corresponding graphs for case 2 (dashed lines). With disabled autoregulation, both scenarios produce similar results below an ABP of $\sim ABP \leq 127$ (hPa). For a higher ABP, the graphs differ, however. Again the $TiPO_2$ shows small differences only. Above an ABP of $\sim ABP > 127$ (hPa), the increase of $TiPO_2$ for case 4 is smaller than for case 2, and the difference between both scenarios increases with a raising ABP.

As before, a larger difference is seen in the ICP response. In cases of a brain swelling, the ICP increases much faster with a raising ABP than in the no swelling case. For an ABP above $ABP > 127$ (hPa), the increase of ICP in the swelling case is nearly twice as fast as for case 2.

B. esHOM

Using the esHOM model, the ICP and $TiPO_2$ dynamics resembles coarsely the HOM model predictions. But here, due to the splitting into two hemispheres, and the incorporation of the Starling resistor in the venous compartments, the influence of a brain swelling has a stronger impact on both the ICP and $TiPO_2$ dynamics, although the ABP interval, where the dynamics are altered, remains principally the same.

In the case of a functioning autoregulation (Fig. 4), the ICP reaches a higher maximal level in the esHOM model than for the HOM model. Additionally, the maximum in ICP occurs at a higher ABP value. On the other hand, the drop in $TiPO_2$ is more pronounced and is observed around an ABP of 120 (hPa). The most significant difference between both models is founded in the response of the $TiPO_2$ to ABP values lower than 120 (hPa). After the drop, the $TiPO_2$ decreases nearly linearly until ABP values lower than 67 (hPa) are reached. Beyond the upper end of this linear increase there is an interval, although very small, where $TiPO_2$ increases while ICP decreases both in a roughly linear manner. As will be shown later, such a behavior can be detected in measurements of the above mentioned neurosurgical multimodal monitoring (see [21]).

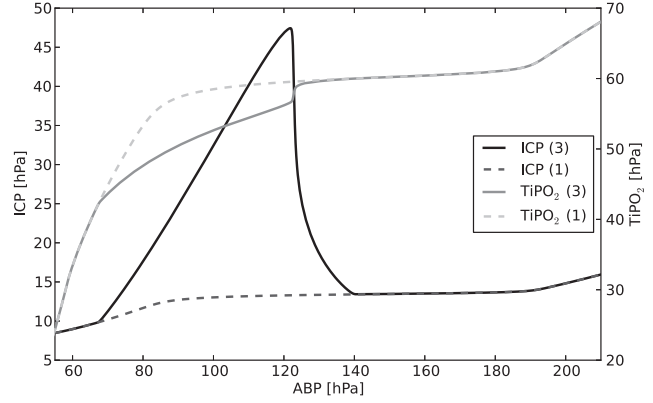


FIG. 4. $TiPO_2$ and ICP against ABP for $\alpha = 2.0$, $V_E = 0$ (ml) (case 1) and $V_E = 30$ (ml) (case 3); esHOM.

In the case of a disabled autoregulation mechanism (Fig. 5), the increase in ICP is around three times faster in the case of a brain swelling than without any swelling. In contrast, the HOM simulation just yields an increase in ICP of two times faster, roughly. The increase of $TiPO_2$ is less pronounced, when compared with the HOM model (see Fig. 3), resulting in an even larger gap between both scenarios.

C. Physiological interpretation

Looking at the behavior of the different compartments, the above mentioned simulation results can be interpreted in the following way: During brain swelling, ABP intervals exist where the CSF compartment is completely depleted, hence no further CSF fluid can be absorbed which leads to a diminished cerebral compliance. In this case, an intact autoregulation in combination with a decreasing ABP induces a dilation of the arterial vessels which in turn leads to an increasing ICP, until the maximal dilation according to the autoregulation is reached. This effect appears much more pronounced with the esHOM model. The inclusion of the Starling resistor, which implies a deformable venous compartment, has a pronounced impact on the venous resistance, and, accordingly, on the global CBF. This distinct influence on the CBF leads to an almost linear decrease of $TiPO_2$ for ABPs in the range 67 (hPa) $\leq ABP \leq 120$ (hPa).

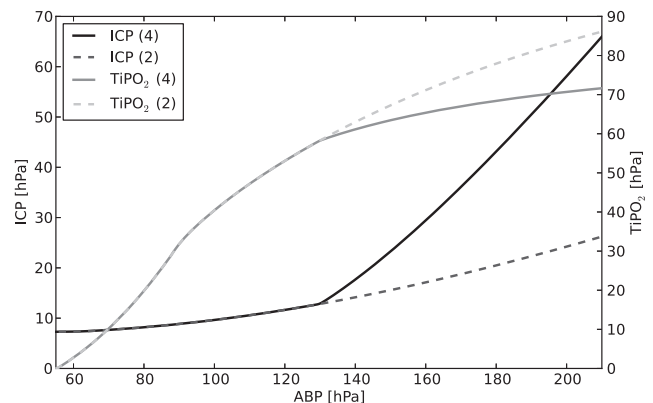


FIG. 5. $TiPO_2$ and ICP against ABP for $\alpha = 0.0$, $V_E = 0$ (ml) (case 2) and $V_E = 30$ (ml) (case 4); esHOM.

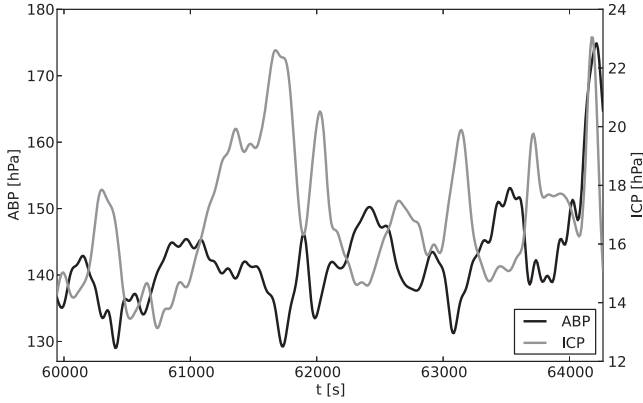


FIG. 6. ABP and ICP against time (measured data).

In sections where CSF fluid can still be absorbed, no significant differences are seen between the simulation results of both models, with or without a brain swelling. Hence, the depletion of the CSF compartment appears to be the critical parameter driving the vastly different behavior of the autoregulation in both scenarios.

V. VALIDATION

To validate the applicability of the HOM model and its extension, the esHOM model, simulation results of their responses are checked against experimental recordings of ICP and $TiPO_2$ within a time window chosen to exhibit pronounced correlations and anticorrelations between the measured physiological parameters.

Specifically, the time window is chosen such that a special case occurs where the ABP is anticorrelated with the ICP, indicating a diminished cerebral compliance caused by a severe brain swelling [21]. This abnormal behavior is illustrated in Fig. 6. Moreover, during this time segment, the ABP is additionally correlated with the $TiPO_2$ as is shown in Fig. 7. A preliminary analysis indicated that this anticorrelation occurs in more than 80% of the patients during neuromonitoring in an intensive care unit, and therefore seems to play a crucial role during the treatment of a severe head trauma.

The depicted graphs represent a low pass filtered version of the original data, simply eliminating certain fast oscillatory components (see [23]).

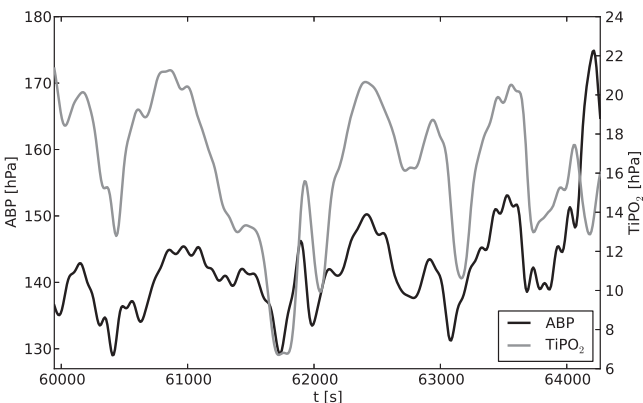


FIG. 7. ABP and $TiPO_2$ against time (measured data).

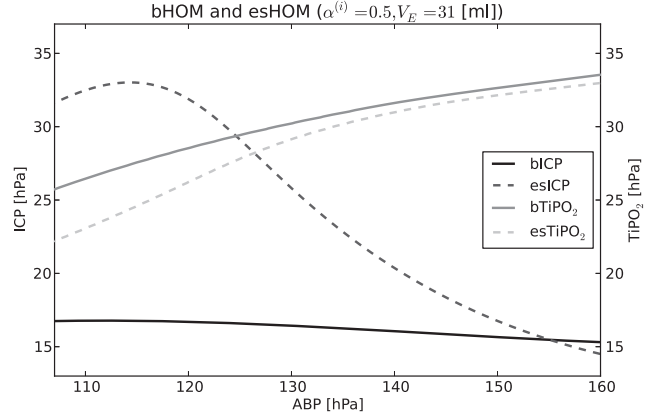


FIG. 8. ICP and $TiPO_2$ against ABP for $\alpha^{(i)} = 0.5$ and $V_E = 31$ (ml) (HOM and esHOM).

From a modeling point of view, the behavior seen in Fig. 6 represents case 3, whereas with case 4 the pronounced positive correlation between ABP and $TiPO_2$ depicted in Fig. 7 is reproduced. Consequently, simulating measured data with the esHOM model, a mixture of case 3 and case 4 has to be assumed. A positive correlation can only be achieved in such simulations if a severe brain swelling meets an active autoregulation. Therefore, we choose to simulate a diminished autoregulation in order to achieve, in addition, a positive correlation between ABP and $TiPO_2$. Within a simulation, a diminished autoregulation can be achieved by adjusting the control parameter α .

A. Simulation with both models

By analyzing the graphs depicted in Fig. 8, simulated with the HOM model (and marked with the prefix “b”), the aforementioned behavior of measured data cannot be reproduced quantitatively. Although a negative correlation is already predicted, the quantitative variation of the ICP is far too small. Increasing α would increase the ICP range, but then the variation in $TiPO_2$ would be reduced. For a smaller value for α , the variation of $TiPO_2$ would increase, but the ICP range would decrease. In conclusion the variation of α within the HOM model reproduces the observations qualitatively, but cannot provide a quantitatively satisfying picture of the experimentally observed pressure variations of the monitored response variables.

The model response can be improved, however, by extending it to include two hemispheres and a Starling resistor, as is done in the esHOM model. The difference between the responses of the HOM and the esHOM models are depicted in Fig. 8 (graphs for the esHOM are prefixed with “es”). Concerning the ICP, there is a significant difference between both models, contrary to the $TiPO_2$ dynamics. This difference between both models originates from different volume dynamics of the blood vessel system. With an enlarged volume of the blood vessel system, the ICP is increased, too, and, analogously, decreased when the volume of the blood vessels decreases.

Now, assuming an intact autoregulation in one hemisphere, but a diminished autoregulation in the other, the sought-after

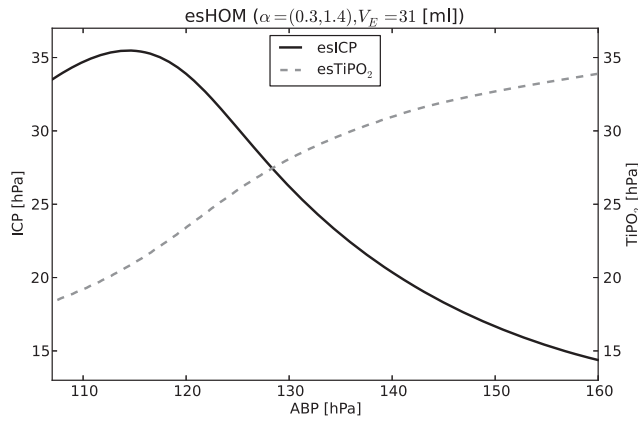


FIG. 9. ICP and $TiPO_2$ against ABP for $\alpha^L = 0.3$, $\alpha^R = 1.4$, and $V_E = 31$ (ml) (esHOM).

effect can be further emphasized as is shown in Fig. 9. With this parameter configuration, the observed correlations and anticorrelations in measured response parameters can be described both qualitatively and quantitatively.

B. Interpretation

With the help of the simulation model, it is possible to interpret the experimentally observed behavior: Due to brain swelling, the CSF compartment is completely depleted in a certain range of ABPs. Therefore, for a decreasing ABP the autoregulation mechanism stabilizes the CBF as far as possible on the basis of its constrained mode of operation. Because of the resulting volume increase of the arteries, the total volume of the blood vessel system grows. But this volume increase cannot be compensated by the CSF compartment, as, due to the brain swelling, it is already completely depleted. Blood volume increase and CSF depletion thus results in a more compressed brain tissue and, therefore, in an increase of the ICP. With a further decrease of the ABP, this effect is amplified and ultimately results in an increase of the ICP with a decreasing ABP. This explains the frequently observed anticorrelation between ICP as the response variable and ABP as the driving force. Additionally, the rising ICP influences the cerebral blood flow via the Starling resistor mechanism. Due to an elevated cerebral vascular resistance, CBF is reduced, leading to a decreasing $TiPO_2$.

VI. CONCLUSION

The dysfunction of cerebral regulatory systems, as cerebral autoregulation or cerebral compliance, may have a dramatic impact on the health status of patients suffering from a severe head trauma. To identify such failures by means of multimodal neuromonitoring data, a mathematical model was introduced to predict the interdependencies between these data in the above mentioned case of failing regulatory systems.

The simple HOM model is able to reproduce experimental behavior as the well known autoregulation curve. Additionally, it predicts different forms of correlations between ABP and ICP in cases of diminished compliance and intact or failing autoregulation in a qualitatively correct way.

But the predictions with the HOM model were shown to be quantitatively incorrect. Furthermore, the HOM model is unable to reproduce a specific combination of correlations where ABP and ICP appear anticorrelated but ABP and $TiPO_2$ appear correlated, a constellation which is observed in about 80% of neuromonitoring recordings from patients suffering from a severe head trauma. To reproduce these striking correlations, two extensions to the HOM model have been introduced:

(1) First, the representation of the elastic venous compartment via a Starling resistor, which increases the influence of a diminished compliance on the cerebral perfusion.

(2) Second, a splitting of the cerebral compartment into two hemispheres with individual autoregulation.

This extended model, called the esHOM model, is able to even quantitatively reproduce the above mentioned scenario of simultaneous correlations and anticorrelations of the multimodal monitoring data. Both modifications have to be used:

(1) The Starling resistor mechanism is responsible for an extended influence of the compliance on the cerebral perfusion promoting a negative correlation between ICP and $TiPO_2$.

(2) Reproducing the experimentally observed behavior quantitatively also affords the inclusion of two distinct hemispheres with independent autoregulation systems to allow for local failures of only one of them.

In summary, the esHOM model can be used as a basis for offline and online analyses, and also for an interpretation of physiological parameters recorded during neuromonitoring.

ACKNOWLEDGMENTS

Financial support by the German Science Foundation (DFG) within the graduate college GK 638 is gratefully acknowledged.

[1] A. Marmarou, Ph.D. thesis, Drexel University, 1973.
 [2] A. Marmarou, K. Shulman, and R. M. Rosende, *J. Neurosurg.* **48**, 332 (1978).
 [3] M. Ursino, *Ann. Biomed. Eng.* **16**, 379 (1988).
 [4] M. Ursino, *Ann. Biomed. Eng.* **16**, 403 (1988).
 [5] M. Ursino and C. A. Lodi, *J. Appl. Physiol.* **82**, 1256 (1997).
 [6] M. Ursino, C. A. Lodi, S. Rossi, and N. Stocchetti, *J. Appl. Physiol.* **82**, 1270 (1997).

[7] M. Ursino and C. A. Lodi, *Am. J. Physiol.* **274**, H1715 (1998).
 [8] M. Ursino, A. Ter Minassian, C. A. Lodi, and L. Beydon, *Am. J. Physiol.* **279**, H2439 (2000).
 [9] M. Banaji, I. Tachtsidis, D. Delpy, and S. Baigent, *Math. Biosci.* **194**, 125 (2005).
 [10] I. Tachtsidis, Ph.D. thesis, University of London, 2005.
 [11] W. D. Lakin, S. A. Stevens, B. I. Tranmer, and P. L. Penar, *J. Math. Biol.* **46**, 347 (2003).

- [12] W. Wakeland and B. Goldstein, *Comput. Biol. Med.* **38**, 1024 (2008).
- [13] A. A. Linninger, M. Xenos, B. Sweetman, S. Ponkshe, X. Guo, and R. Penn, *J. Math. Biol.* **59**, 729 (2009).
- [14] N. J. Pelc, R. J. Herfkens, A. Shimakawa, and D. R. Enzmann, *Magn. Reson. Q* **7**, 229 (1991).
- [15] Iain K. Moppett and Jonathan G. Hardman, *Anesth. Analg., Hagerstown, MD, US* **105**, 1094 (2007).
- [16] N. Masoumi, D. Bastani, S. Najarian, F. Ganji, F. Farmanzad, and A. S. Seddighi, *IEEE Trans. Biomed. Eng.* **57**, 1255 (2010).
- [17] B. Sweetmana, M. Xenos, L. Zitella, and A. A. Linninger, *Comput. Biol. Med.* **41**, 67 (2011).
- [18] M. C. Aoi, B. J. Matzuka, and M. S. Olufsen, *Conf. Proc. IEEE Eng. Med. Biol. Soc.* **2011**, 2410 (2011).
- [19] F. M. Kashif, G. C. Verghesel, V. Novak, M. Czosnyka, and Th. Heldt, *Sci. Transl. Med.* **4**, 129ra44 (2012).
- [20] A. Jung, R. Faltermeier, R. Rothhoerl, and A. Brawanski, *J. Math. Biol.* **51**, 491 (2005).
- [21] Rupert Faltermeier, Martin A. Proescholdt, and Alexander Brawanski, *Acta Neurochir. Suppl.* **114**, 35 (2012).
- [22] A. Zeiler, R. Faltermeier, M. Böhm, I. R. Keck, A. M. Tomé, C. G. Puntonet, A. Brawanski, and E. W. Lang, *Empirical Mode Decomposition Techniques for Biomedical Time Series Analysis* (Bentham Publishers, Hilversum, 2010), Chap. 4, pp. 60–81.
- [23] A. Brawanski, R. Faltermeier, R. D. Rotherl, and C. Woertgen, *J. Cerebral Blood Flow Metab.* **22**, 605 (2002).